Anomalous columnar order of charged colloidal platelets

ARTICLE *in* THE JOURNAL OF CHEMICAL PHYSICS · JANUARY 2012

Impact Factor: 2.95 · DOI: 10.1063/1.3673877 · Source: PubMed

4 AUTHORS, INCLUDING:

Rik Wensink
French National Centre for Scientific Research
46 PUBLICATIONS **995** CITATIONS
SEE PROFILE

Alejandro gil-villegas
Universidad de Guanajuato
78 PUBLICATIONS **2,017** CITATIONS
SEE PROFILE

Anomalous columnar order of charged colloidal platelets

L. Morales-Anda, H. H. Wensink, A. Galindo, and A. Gil-Villegas

Citation: J. Chem. Phys. **136**, 034901 (2012); doi: 10.1063/1.3673877
View online: http://dx.doi.org/10.1063/1.3673877
View Table of Contents: http://jcp.aip.org/resource/1/JCPSA6/v136/i3
Published by the AIP Publishing LLC.

Anomalous columnar order of charged colloidal platelets

L. Morales-Anda,[1] H. H. Wensink,[2] A. Galindo,[3] and A. Gil-Villegas[1,a)]
[1]*Departamento de Ingeniería Física, División de Ciencias e Ingenierías Campus León, Universidad de Guanajuato, Colonia Lomas del Campestre, León 37150, México*
[2]*Institute for Theoretical Physics: Soft Matter, Heinrich-Heine-University-Düsseldorf, Universitätsstraße 1, 40225, Düsseldorf, Germany*
[3]*Department of Chemical Engineering, Imperial College London, South Kensington Campus, London SW7 2AZ, United Kingdom*

(Received 4 September 2011; accepted 12 December 2011; published online 17 January 2012)

Monte Carlo computer simulations are carried out for a model system of like-charged colloidal platelets in the isothermal-isobaric ensemble (NpT). The aim is to elucidate the role of electrostatic interactions on the structure of synthetic clay systems at high particle densities. Short-range repulsions between particles are described by a suitable hard-core model representing a discotic particle. This potential is supplemented with an electrostatic potential based on a Yukawa model for the screened Coulombic potential between infinitely thin disklike macro-ions. The particle aspect-ratio and electrostatic parameters were chosen to mimic an aqueous dispersion of thin, like-charged, rigid colloidal platelets at finite salt concentration. An examination of the fluid phase diagram reveals a marked shift in the isotropic-nematic transition compared to the hard cut-sphere reference system. Several statistical functions, such as the pair correlation function for the center-of-mass coordinates and structure factor, are obtained to characterize the structural organization of the platelets phases. At low salinity and high osmotic pressure we observe anomalous hexagonal columnar structures characterized by interpenetrating columns with a typical intercolumnar distance corresponding to about half of that of a regular columnar phase. Increasing the ionic strength leads to the formation of glassy, disordered structures consisting of compact clusters of platelets stacked into finite-sized columns. These so-called "nematic columnar" structures have been recently observed in systems of charge-stabilized gibbsite platelets. Our findings are corroborated by an analysis of the static structure factor from a simple density functional theory. [doi:10.1063/1.3673877]

I. INTRODUCTION

The liquid crystal phase behavior of hard discotic colloidal particles has been studied both from computer simulation, using simplified models,[1–4] and experiments on sterically stabilized discotic model colloids.[5] The possibility of a first order disorder-order transition from an isotropic to a discotic nematic fluid was first established theoretically by Onsager[6] in the late 1940s. Although originally devised for rod-like particles in solution, his theory also makes qualitative predictions for plate-like particles based on the central idea that orientation-dependent steep repulsive interactions alone are responsible for stabilizing nematic order. At high densities a stable columnar phase is formed which is characterized by a two-dimensional lattice of columns with a liquid-like internal structure. The study of the phase behavior of hard discotic particles with variable particle shape has been the subject of recent simulation[7–10] and theoretical work.[11]

Most discotic colloidal systems (notably clays) consist of charged disk- or sheetlike mesogens.[12] The disposition of surface charges of clay particles can be very complicated as the chemical composition of the edge surfaces tends to be different from that of the flat surfaces. Further complications arise from the fact that the particle dimensions and surface charge densities are strongly non-uniform. The considerable polydispersity in size, charge, and composition inherent to clay systems has restricted its fundamental study.[12]

The subtle balance between the attractive van der Waals forces which are dominant at short interparticle distances and the repulsive electrostatic forces at large distances may give rise to a rich variety of rheological behavior, ranging from simple Newtonian to viscoelastic flow. This transition from one rheological state to the other is intimately coupled to changes in the microstructure of the clay particles due to gelation or swelling of the lamellar structure which can be brought about by changing the ionic strength of the solution.[13,14] The microstructure of clay suspensions has been investigated in a number of computer simulation studies in which coarse-grained interaction site models have been employed to describe the low-density dynamics[15] and gelation of laponite clays.[16–19] In Ref. 20 an explicit Coulombic site model has been used to examine gel formation of kaolin clays. Within the context of molecular discotic liquid crystals, a similar projection of the molecular details onto coarse-grained point-charge models has proven useful.[21]

Most of the numerical studies on model clay particles to date focus on the low-density isotropic fluid state. The effect of electrostatic interactions on the stability of the various liquid crystalline phases (nematic, columnar) remains elusive for many natural clay systems as the formation of these

a)Electronic mail: gil@fisica.ugto.mx.

structures tends to be pre-empted by gelation.[13] Examples of clays which do exhibit isotropic-nematic transitions are natural nontronite[22] and beidelite,[23] synthetic gibbsite,[24] and mixed metal hydroxides.[25] Thermodynamically stable columnar phases have been observed in systems of nickel(II) hydroxide[26] and gibbsite[24] platelets. Synthetic gibbsite clays thus display the full sequence of liquid crystal phases predicted by the hard-particle models.[1,6] The impact of electrostatic interactions on the formation of dense liquid crystalline phases (such as the columnar one) and glasses in gibbsite clays is an area of recent investigation.[27–29] The relative strength of the dispersion and electrostatic interactions in these systems can be carefully tuned by varying the ionic strength of the solvent. At high ionic strength the gibbsite systems develop a gel state whereas at low ionic strength a repulsive glass with a "columnar nematic" structure is observed. The latter consists of a disordered collection of short columnar stacks with strong orientational order.[30]

These recent observations in synthetic clay systems provide experimental stimulus for undertaking a numerical study of like-charged clay particles at particle densities going beyond the low-density isotropic fluid regime considered thus far. The main focus of this project is to scrutinize the structure and phase behavior of like-charged rigid discotic colloidal particles at arbitrary densities by means of Monte Carlo computer simulation. Our approach is based on a simple, coarse-grained Yukawa potential for the screened-electrostatic interactions. Short-range correlations between the platelets are captured by a hard-core repulsion embodied by a simple cut-sphere shape. More explicit models for non-isometric macro-ions based on explicit ion-ion correlations have been considered for oppositely charged oblate particles[31] and for charged spherocylinders.[32–34] However, due to the large number of charged sites residing on the surface of a mineral discotic colloid, an effective potential is introduced via the Yukawa model. The effective surface charge of a clay particle will depend on the degree of counterion-condensation on the particle surface and is expected to be in the range 10–100e.

This paper is structured as follows: In Sec. II we introduce the hard-core Yukawa model for charged discotic particles mentioned above, followed by a brief exposition of the simulation methodology in Sec. III. Results for the low-density isotropic and nematic fluid phases are shown in Sec. IV A. The implications of the electrostatic interactions on the high-density structures are discussed in Sec. IV B. A theoretical analysis of the nematic-columnar transition based on the static structure factor of charged platelets is presented in Sec. IV C. Finally, Sec. V is devoted to a discussion and some concluding remarks.

II. HARD-CORE YUKAWA MODEL FOR CHARGED COLLOIDAL PLATELETS

In this work we shall examine the effect of electrostatic interactions between the platelets starting from a continuum electrostatic model based on a screened Coulombic potential. A detailed discussion of the electrostatic potential of discotic macro-ions within the nonlinear Poisson-Boltzmann (PB) theory has been given in Ref. 35. The main finding is that the nonlinear screening effects allow us to treat the charged disks as an effective system which can subsequently be analyzed within the linear Poisson-Boltzmann theory. This leads to a reliable expression for the *far-field* behavior between two macro-ions with a discotic or any arbitrary shape, as analyzed in Ref. 36 for thin charged rod-like cylinders.

Within linearized PB theory the electrostatic interaction between two point macro-ions with equal charge $\pm Ze$ in a dielectric solvent with relative permittivity ε_r is given by[37]

$$\beta U_Y(r) = Z^2 \lambda_B \frac{\exp[-\kappa r]}{r}, \tag{1}$$

where r is the center-center distance between the macro-ions, $\lambda_B = e^2/4\pi\varepsilon_0\varepsilon_r k_B T$ is the Bjerrum length, where ε_0 is the dielectric permittivity in vacuum ($\lambda_B = 0.7$ nm for water at $T = 298$ K) and κ denotes the Debye screening constant which measures the extent of the *electric double layer* surrounding each particle. In case of excess added salt the screening constant can be written as[38]

$$\kappa = \sqrt{8\pi\lambda_B (N_{av}/1000) c_{salt}} \tag{2}$$

with N_{av} Avogadro's number and c_{salt} the concentration of added salt (1:1 electrolyte in mol/l).

In recent years, several studies have been reported on the structure of charge-stabilized colloidal dispersions using a Yukawa density-dependent potential.[39–44] This approach is based on the mapping of the multicomponent Hamiltonian for the charged colloidal dispersion onto a one-component model, in which the micro-ions are integrated out of the description and the colloidal particles interact via an effective pair potential. In the Debye-Hückel approach, the Yukawa potential arises naturally as an exact interaction for weakly charged species and linearizing the Poisson-Boltzmann equation. This linearization procedure is no longer valid when we are dealing with strongly charged systems, however, the Yukawa potential still can be used as an effective interaction, with density-dependent parameters or with a variable range.[45] In a previous work, a similar approach was successfully used to simulate asphaltenes aggregation behavior, via an effective Lennard-Jones effective interaction between asphaltenes particles.[46]

For the case of platelets, a general form of the effective Yukawa potential, Eq. (1), can be obtained from linearized PB theory by considering two infinitely thin disk-shaped macro-ions of diameter D at arbitrary orientations, denoted by the orientational unit vectors $\{\hat{\mathbf{u}}_1, \hat{\mathbf{u}}_2\}$, and center-of-mass positions $\{\mathbf{r}_1, \mathbf{r}_2\}$. The corresponding potential can be cast in terms of a double convolution of the screened Coulomb potential over the disk surfaces,[17]

$$\beta U_{YD}(|\mathbf{r}_1 - \mathbf{r}_2|; \hat{\mathbf{u}}_1, \hat{\mathbf{u}}_2) = Z^2 \lambda_B \int d^2\mathbf{s} \int d^2\mathbf{t} \frac{\exp[-\kappa|(\mathbf{r}_1 + \mathbf{s}) - (\mathbf{r}_2 + \mathbf{t})|]}{|(\mathbf{r}_1 + \mathbf{s}) - (\mathbf{r}_2 + \mathbf{t})|}, \tag{3}$$

where $\{\mathbf{s}, \mathbf{t}\}$ are position vectors for points over the disks surfaces. This fourfold integral can be transformed to a more

manageable expression by performing a multi-polar expansion of Eq. (3). This procedure has been outlined in detail in Refs. 17 and 38 and leads to the following *far-field* result, valid for large interparticle distances:

$$\beta U_{YD}(|\mathbf{r}_1-\mathbf{r}_2|;\hat{\mathbf{u}}_1,\hat{\mathbf{u}}_2) \sim \beta U_Y(|\mathbf{r}_1-\mathbf{r}_2|) \times\left[1+\frac{(\kappa D)^2}{32}(\xi_1+\xi_2)+\frac{(\kappa D)^4}{1024} \times\left(\xi_1\xi_2+\frac{1}{3}\xi_1^2\xi_2^2\right)+\mathcal{O}\{(\kappa D)^6\}\right] \tag{4}$$

with $\xi_i = 1-(\hat{\mathbf{r}}\cdot\hat{\mathbf{u}}_i)^2$ and $\hat{\mathbf{r}} = (\mathbf{r}_1-\mathbf{r}_2)/|\mathbf{r}_1-\mathbf{r}_2|$ the center-of-mass distance unit vector. Equation (4) includes all contributions up to the monopole-hexadecapole interactions. The orientation-dependent pair potential Eq. (4) is minimized if the two disks are both parallel and coaxial ($\xi_1 = \xi_2 = 0$). The approximate Yukawa potential can, in principle, be generalized to include multi-polar contributions of higher order by extending the Taylor expansion of the *exact* far-field result up to higher terms in κD.[17] The expansion in Eq. (4) is expedient because of its numerical simplicity while being sufficiently accurate for moderately screened systems ($1 < \kappa D < 10$) studied in this paper. We remark that Eq. (4) is only valid if $\kappa|\mathbf{r}_1-\mathbf{r}_2| \gg 1$ so it becomes less reliable at high colloid densities where the average particle distance is no longer sufficiently large. Moreover, contributions due to nonlinear screening (which can be quantified from the nonlinear PB equation) will come into play and influence particle correlations at short distances.[35] Despite these shortcomings we assume that the potential in Eq. (4) is able to provide qualitative insight into the microstructure of charged disks at arbitrary densities provided that the short-range correlations are accounted for in an effective way, an approach that has given accurate predictions on the case of asphaltene systems.[46]

The dominant contribution to the particle interactions at short distances is likely to stem from the steric interactions associated with the (effective) particle shape. The analysis of the linearized PB equation is restricted to particles with vanishing internal volume (infinitely thin disks) and its extension towards objects with a finite volume is non-trivial.[17] In order to account for the finite thickness of the platelets we shall combine the electrostatic potential with a suitable hard-core model which represents the intrinsic shape of the colloid. The hard-core contribution to the total potential will capture the steep repulsive interactions (due to both steric effects and nonlinear screening) prevalent at short particle interparticle distances.

In the so-called *hard cut-sphere* (HCS) model a discotic colloid is represented by a truncated sphere, which can be constructed by slicing off the end-caps of a sphere of diameter D at a distance $L/2$ from the equator.[2] In this way, a disk-like object is obtained with an *aspect-ratio* L/D interpolating between that of an infinitely thin disk ($L/D = 0$) and a sphere ($L/D = 1$). The total potential is now given by

$$\beta U(|\mathbf{r}_1-\mathbf{r}_2|;\hat{\mathbf{u}}_1,\hat{\mathbf{u}}_2) = \begin{cases}\infty & |\mathbf{r}_1-\mathbf{r}_2| \le \sigma(\hat{\mathbf{r}};\hat{\mathbf{u}}_1,\hat{\mathbf{u}}_2)\\ \beta U_{YD}(|\mathbf{r}_1-\mathbf{r}_2|;\hat{\mathbf{u}}_1,\hat{\mathbf{u}}_2) & |\mathbf{r}_1-\mathbf{r}_2| > \sigma(\hat{\mathbf{r}};\hat{\mathbf{u}}_1,\hat{\mathbf{u}}_2)\end{cases} \tag{5}$$

with $\sigma(\hat{\mathbf{r}};\hat{\mathbf{u}}_1,\hat{\mathbf{u}}_2)$ the center-of-mass contact distance between two cut-spheres at a given set of orientational unit vectors. The phase behavior of the hard cut-sphere reference system has been addressed in a number of simulation studies.[1,2,7,47–49]

III. SIMULATION DETAILS

Standard Monte Carlo simulations in the isobaric-isothermal (NpT) ensemble have been employed to obtain the equilibrium structures as a function of density for a given pressure p, room temperature $T = 298$ K, and electrostatic parameters (surface charge Z, Bjerrum length λ_B, and electrostatic screening constant κ). Details for the overlap routine for HCS can be found in Ref. 50. Simulations are based on $N = 1000$ particles in a three-dimensional simulation box with periodic boundary conditions in all directions. The box was taken to be cubic in case of fluid phases at low pressure, however, ordered structures emerging at high pressure may be incommensurate with the periodic boundary conditions if a cubic simulation cell is used. We therefore allowed the Cartesian box dimensions to vary independently in such cases. The equations-of-state are determined by compression runs starting from a random, isotropic configuration of non-overlapping HCS. At high pressure, simulation runs were carried out using a nematic initial configuration of randomly positioned, perfectly aligned platelets.

In order to speed up the calculation of the potential energy of the system Verlet lists were used which keep track of particles located within a certain cutoff-range r_c for the Yukawa potential. Throughout the study we have fixed $r_c = 7\kappa^{-1}$. Each simulation run consists of an equilibrium run of at least $1–2 \times 10^6$ Monte Carlo cycles and a production run in which data were collected and averaged over typically 1×10^6 cycles. The magnitude of the trial moves (translation, rotation, and volume perturbation) was chosen adaptively so as to maintain an overall acceptance ratio of about 50%.

IV. RESULTS

A. Isotropic and nematic fluid phases

First, we have examined the phase diagram of a reference system of hard-cut spheres. The phase behavior of HCSs with a given aspect-ratio L/D only depends on the particle density $c = ND^3/V$ or packing fraction ϕ, defined as

$$\phi = c\frac{\pi}{12}\left(\frac{L}{D}\right)\left[3-\left(\frac{L}{D}\right)^2\right] \tag{6}$$

and is known to feature an isotropic-nematic transition at low densities. A key parameter to distinguish between these two states is the nematic order parameter S which, for a common uniaxial nematic phase, is defined as the maximum eigenvalue of the second-rank tensor,

$$\mathbf{Q} = \frac{1}{N}\left(\sum_i^N \frac{3}{2}\langle\hat{\mathbf{u}}_i\otimes\hat{\mathbf{u}}_i\rangle - \frac{1}{2}\mathbf{I}\right), \tag{7}$$

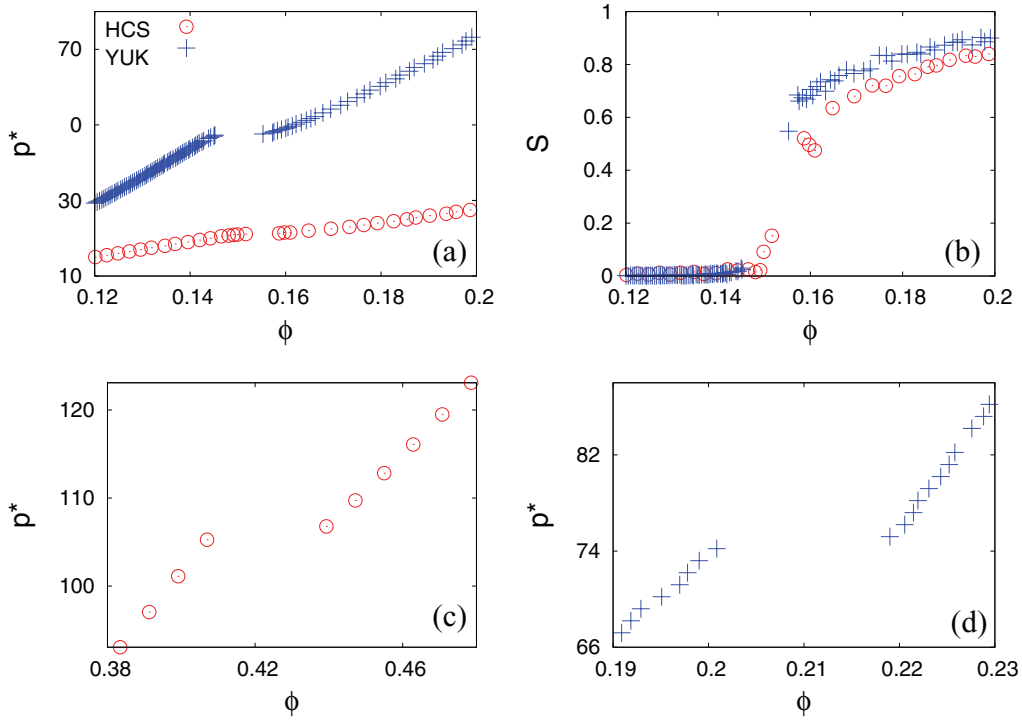

FIG. 1. (a) Phase diagram of a system of $N = 1000$ Yukawa cut-spheres (YUK) of aspect-ratio $L/D = 0.05$ compared to that of the hard cut-spheres reference system (HCS). Plotted is the system pressure $p^* = \beta p D^3$ versus the volume fraction ϕ. The corresponding nematic order parameter S is shown in (b). The parameters for the Yukawa system are: $Z = 100$, $c_{salt} = 10^{-4}$ M, $\lambda_B/D = 0.00233$, and $\kappa D = 9.76$. (c) High-density regime featuring a first-order phase transition from a nematic to a columnar phase of hard cut-spheres. (d) Same for Yukawa disks.

where $\otimes$ denotes the dyadic product, $\mathbf{I}$ represents the unit second-rank tensor, and $\langle \cdot \rangle$ denotes a canonical average. The equation-of-state in Fig. 1 exhibits an isotropic-nematic transition around scaled pressure $\beta p D^3 \approx 21.1 \pm 0.2$. The transition is found to be weakly first order with a small density jump occurring around $ND^3/V \approx 4$ accompanied by a moderate jump ($S \approx 0.5 \pm 0.03$) in the nematic order parameter, in good agreement with the data presented in Ref. 48.

We evaluated the pressure versus density of a system of $N = 1000$ Yukawa platelets of $L/D = 0.05$. Since at any given density the dynamics of the Yukawa particles is generally slower than that of the HCS reference system, care is taken to ensure proper equilibration at each pressure step. Typically 2×10^6 cycles are needed for each equilibration step and another 1×10^6 cycles for calculating the observables. The resulting equation-of-state for a system of Yukawa disks with surface charge $Z = 100$ at salt concentration $c_{salt} = 10^{-4}$ M is shown in Fig. 1 and features a similar isotropic-nematic transition albeit at a much higher coexistence pressure $\beta p D^3 = 47.2 \pm 0.2$. The phase transition of the Yukawa disks appears more strongly first-order, both in terms of the particle density and nematic order parameter. The transition densities do not differ drastically from that of the HCS system but has shifted to somewhat lower densities ($c_I \approx 3.7$, $c_N \approx 4$).

For charged colloidal systems it is customary to account for the double-layer repulsions between the particles by mapping the electrostatic potential onto a hard-core one with an *effective* shape determined by the thickness of the electrical double layer. As for the disks one may naively propose a set of effective dimensions $\bar{L} \to L + 2/\kappa$, and $\bar{D} \to D + 2/\kappa$. Likewise, the pressure concentration and aspect-ratio can be rescaled as follows:

$$\begin{aligned} \beta p \bar{D}^3 &\to \beta p D^3 \epsilon^3 \\ \bar{c} &\to c\epsilon^3 \\ \frac{\bar{L}}{\bar{D}} &\to \frac{1}{\epsilon}\left(\frac{L}{D} - 1 + \epsilon\right), \end{aligned} \tag{8}$$

where $\epsilon = 1 + 2(\kappa D)^{-1}$. For the systems considered here $\epsilon \approx 1.205$ and the rescaling would lead to an effective aspect-ratio of $\bar{L}/\bar{D} \approx 0.21$ in which case nematic order tends to be suppressed in favour of cubatic order.[2,7] Moreover, the coexistence pressure for the charged system would be underestimated by Eq. (8). This implies that the shift in the isotropic-nematic coexistence properties observed in Fig. 1 does not follow the simple scaling prescription suggested by Eq. (8).

Microscopic information regarding the positional structure of the various phases can be analyzed from the pair correlation function $g(r)$ for the center-of-mass position,

$$g(r) = \frac{1}{N}\left\langle \frac{1}{\rho} \sum_{i,j=1;i\neq j}^{N} \delta(r - |\mathbf{r}_i - \mathbf{r}_j|) \right\rangle, \tag{9}$$

where the brackets denote a canonical average. The orientational pair correlations are routinely measured by the function,[51]

$$g_P(r) = \frac{1}{Ng(r)}\left\langle \frac{1}{\rho} \sum_{i,j=1;i\neq j}^{N} \mathcal{P}_2(\hat{\mathbf{u}}_i \cdot \hat{\mathbf{u}}_j)\delta(r - |\mathbf{r}_i - \mathbf{r}_j|) \right\rangle, \tag{10}$$

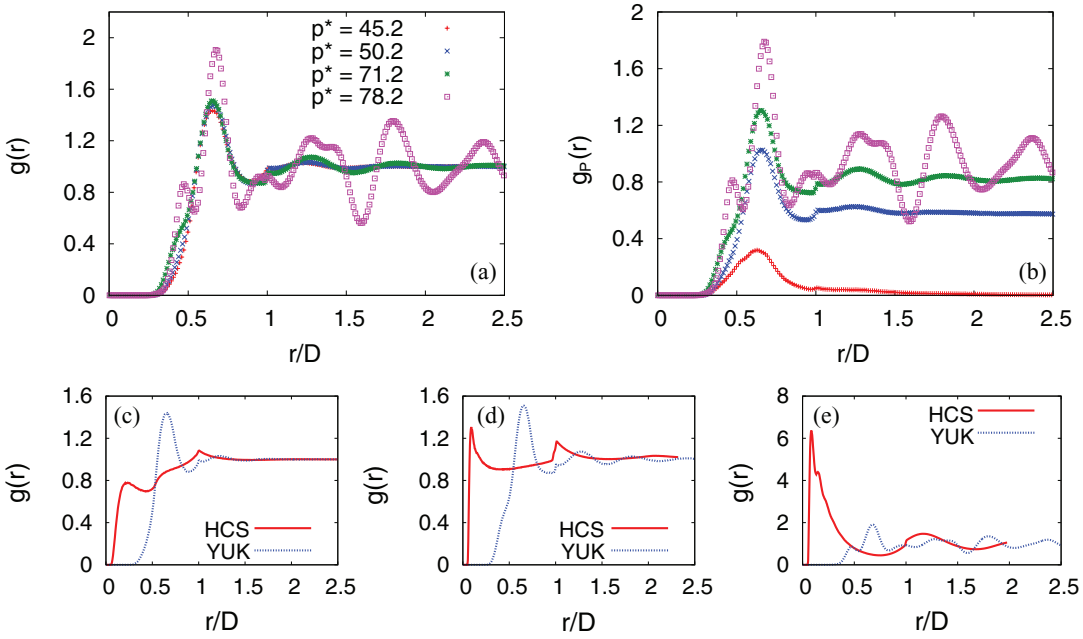

FIG. 2. (a) Pair correlation function for the center-of-mass coordinate of the Yukawa platelets as a function of the center-of-mass distance r measured in units of the plate diameter D. Pressures are expressed as $p^* = \beta p D^3$. The electrostatic parameters are as in Fig. 1. (b) Orientational pair correlation function defined in Eq. (10). Comparison of the pair correlation function for the hard cut-sphere (HCS) and Yukawa platelets (YUK) at a number of state-points: (c) isotropic phase at $p^* = 18$ (HCS), $p^* = 45.2$ (YUK), (d) nematic phase at $p^* = 80$ (HCS), $p^* = 71.2$ (YUK), and (e) columnar phase at $p^* = 150$ (HCS), $p^* = 78.2$ (YUK).

where $\mathcal{P}_2(x) = (3x^2 - 1)/2$ is the second-order Legendre polynomial. At low pressures, corresponding to an isotropic fluid, the center-of-mass pair correlation functions (Fig. 2) exhibit a regular structure with a main peak situated at a typical mean-interparticle distance 0.65 ± 0.01 D. The structure remains rather insensitive to pressure throughout the nematic branch. At very large pressure a much richer correlation function is found with the notable split of the first peak being a hallmark of partial freezing transition. The orientation pair correlations reveal a common decay for the isotropic phase indicating a lack of long-ranged orientational correlations. This situation is different in the nematic phase[50] where $g_P(r)$ levels off to a non-zero plateau value $g_P(r \to \infty) \propto S^2$.

It is instructive to compare the structure of the Yukawa platelets with that of the HCS system at different representative state-points throughout the phase diagram. The results (Fig. 2) clearly demonstrate that the isotropic phase of Yukawa platelets has a more pronounced structure than the HCS at comparable density. Moreover, the microstructure of the nematic phase of HCS is markedly different from that of the isotropic phase. The pronounced correlation peak at small distances which corresponds to the average inter-particle distance along the nematic director, is much weaker in the isotropic phase. The main peak shifts to increasingly lower distances as the pressure increases. This trend contrasts with the observations for the Yukawa system where the positional structure seems to change very little when going from the isotropic to the nematic fluid phase. Here, the main structure peak remains located at about 0.7 times the disk diameter, irrespective of the density.

B. Columnar phases

Additional simulations were carried out in order to investigate stable liquid crystalline structures at high pressure. The central question here is whether the hexagonal columnar structure, as commonly found in dense discotic systems, is retained in case of the presence of the soft repulsive Yukawa potential. The resulting structure is shown in Fig. 3 and reveals a remarkable *interdigitated* hexagonal structure, whereby the platelets adopt liquid-like "roof-tile"-like local arrangements along the column direction. The interpenetration of the adjacent columns is clearly reflected by the static structure factor $S(k)$ (see the Appendix) which exhibits a regular hexagonal pattern of Bragg spots. The average distance between the diffraction spots is $\Delta k D \approx 13$ which corresponds to an intercolumnar spacing of about 0.5 D. The "intracolumnar" structure can be gleaned from $S(k_z)$ (Fig. 3) which appears liquid-like for all three cases shown. The location of the main peak is connected to the average distance between the particles inside the columns which is clearly much larger for the charged platelets than for the hard particles (Fig. 3(c)). The relatively low packing fraction ($\sim$22%) of the ordered structures for the charged case can be explained from the effective shape of the platelets which gives rise to an effective packing fraction (cf. Eq. (8)) higher than the bare one. The interdigitated structures are a consequence of the Yukawa potential Eq. (4) which strongly disfavors face-to-face configurations at short particle distances due to the energy penalty caused by the overlap of the electric double layers.

There are two effects to be considered in relation to Eq. (4). On the one hand, for parallel disks face-to-face pair

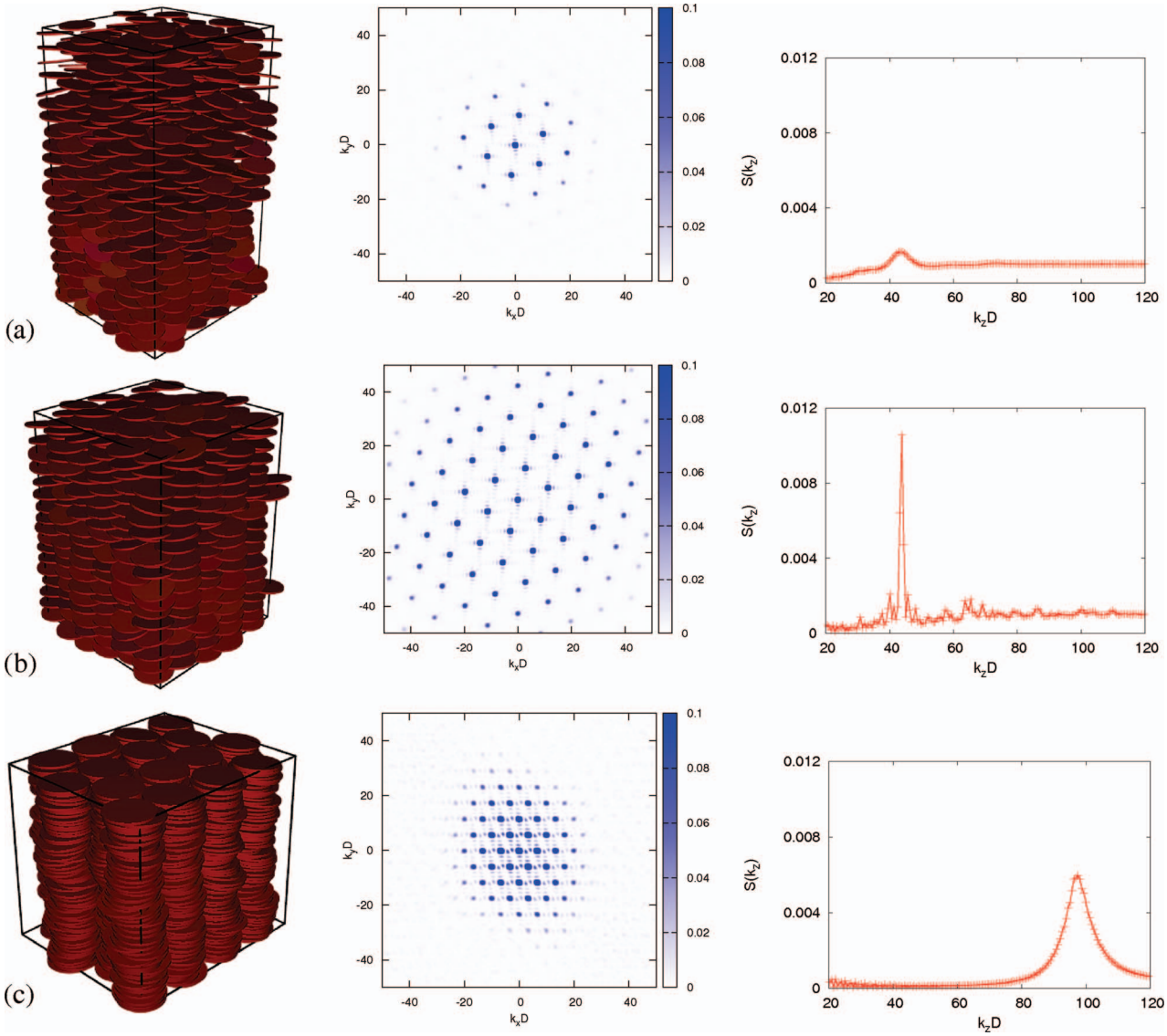

FIG. 3. (a) Snapshot of an interdigitated columnar phase of Yukawa disks formed at $p^* = 85$ with packing fraction $\phi = 0.22$. The aspect-ratio is $L/D = 0.05$, the disk charge is $Z = 100$, and salt concentration is $c_{salt} = 1 \times 10^{-4}$ M. (b) Same system at $p^* = 300$ ($\phi = 0.36$). (c) Regular hexagonal columnar structure of (uncharged) hard cut-spheres at $p^* = 200$ and packing fraction at $\phi = 0.59$. The panels in the middle depict the transverse static structure factor $S(k)$ (Eq. (A1)) showing the xy projection perpendicular to the direction of the columns. The right panels show the structure factor along the columnar direction z.

configurations are favorable over edge-to-face ones by virtue of ξ. On the other hand, edge-to-face configurations (at fixed face-to-face distance) correspond to a larger center-of-mass distance between the disks and thus lead to a reduced potential energy. At high densities where interparticle distances are relatively small the second effect will most probably be dominant and the particles will simply try to be as far apart from each other (hence, favoring edge-face pair configurations). It is important to bear in mind that the structure observed is the result of many-body correlations and not just pair correlations, and is also strongly governed by the orientational and excluded-volume entropy associated with the hard-core part of the pair potential.

The extent of the electrical double-layers can be reduced by increasing the salt concentration of the suspension. This leads to a number of different high density structures shown in Fig. 4. For $c_{salt} = 2 \times 10^{-4}$ M the hexagonal columnar structure is largely retained although signs of local melting are clearly discernible. The degree of disorder becomes much more pronounced for higher salt concentrations where the columnar structure is disrupted in favor of short stacks. This scenario is most clearly visible for the case $c_{salt} = 1 \times 10^{-3}$ M where string-like structures consisting of a strongly aligned platelets are evident. The loss of hexagonal order in favor of a disordered configuration of compact columnar stacks of platelets is reflected in the pair correlation function shown in Fig. 4. At low salt concentrations the main peak is situated at $r/D \sim 0.5$ demarcating the average intercolumnar distance, while the secondary one at smaller distances measures the average *intra*-columnar distance between the platelets inside the columns. Upon increasing the salt concentration the *intra*-columnar peak strongly intensifies at the expense of the intercolumnar peak indicating a break-up of the hexagonal packing of columns into separated compact stacks with a finite length.

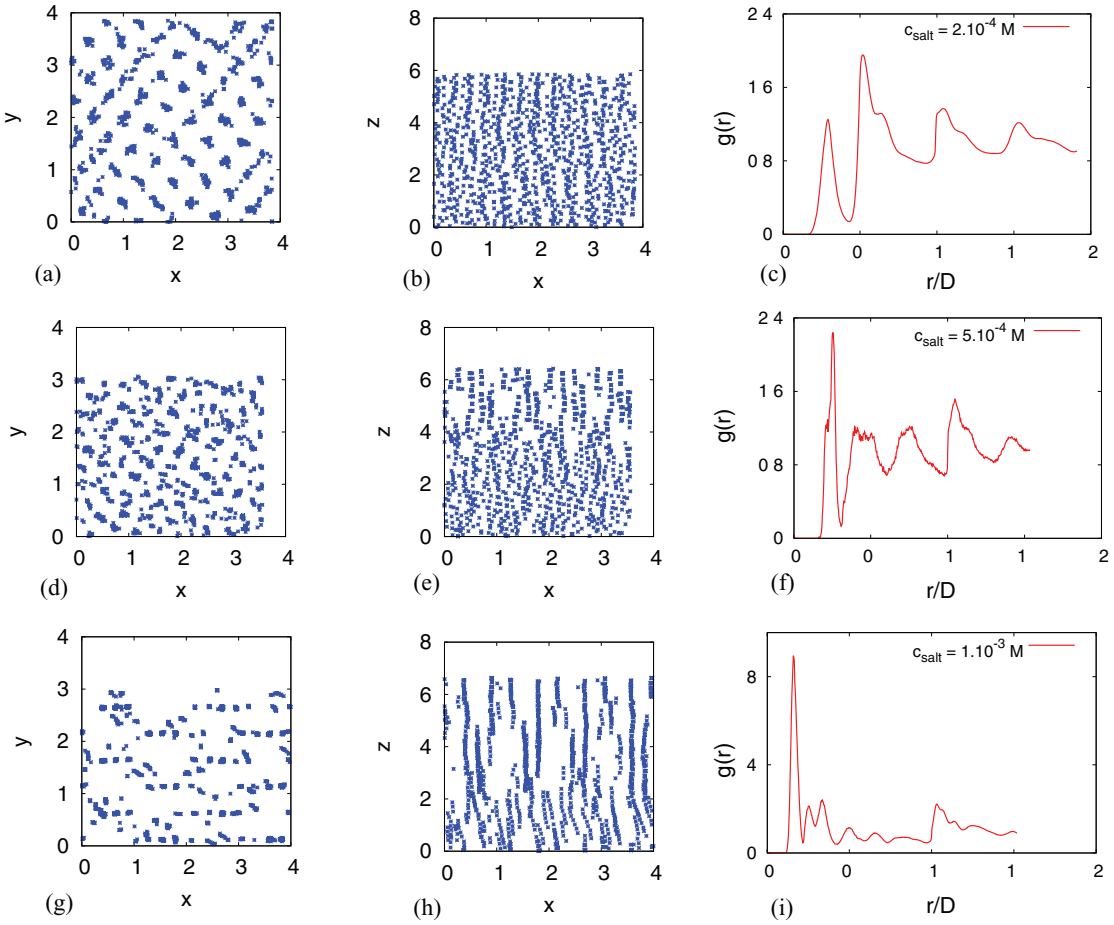

FIG. 4. Snapshots of the center-of-mass coordinates of dense structures of Yukawa platelets of aspect-ratio $L/D = 0.05$, charge $Z = 100$, and salt concentration $c_{salt} = 2 \times 10^{-4}$ M at fixed pressure $p^* = 300$. The projections of the center-of-mass coordinates are shown onto the xy-plane (a), and the xz-plane (b). The pair correlation function is shown in (c). The results for $c_{salt} = 5 \times 10^{-4}$ M are shown in (d)–(f), the ones for $c_{salt} = 1 \times 10^{-3}$ M in (g)–(i). The latter structure is characterized by a disordered string-like configuration of stacked platelets aligned along the z-direction. The packing fractions of the structures are $\phi = 0.45$ (a)–(c), $\phi = 0.56$ (d)–(f), and $\phi = 0.48$ (g)–(i).

To rule out transient effects in the structure formation very long equilibrium runs (up to 1×10^7 MC cycles) were adopted to arrive at stationary configurations. Moreover, two different starting configuration were considered; a fluid state of perfectly aligned platelets and a perfectly ordered face-centered-cubic lattice. Both initial configurations lead to similar structures which are found to be persistent in time with a strongly reduced particle mobility. The structures in Fig. 4 thus strongly resemble dynamically arrested glass states characterized by dynamical heterogeneities, i.e., regions of slow and fast particle mobility. We remark that a regular columnar phase such as the one shown in Fig. 3 is retained in the limit of very high salt concentrations. The effect of the electrostatic repulsions will be negligible if the range of the Yukawa potential (measured by the Debye length) is much smaller than the thickness of the platelet. In experimental situations, high salt concentrations usually lead to a flocculation or gelation of the mineral colloids since the short-range attractive London-van der Waals forces (which are neglected in the present study) become dominant in the regime of strong screening.[30]

Although string phases have been stabilized in dipolar hard spheres fluids, it is difficult for us to confirm the stability or metastability of the phases shown here, as no free-energy calculations were carried out. For dipolar systems the string phase is the ground state ($T = 0$) and is therefore expected to be the thermodynamically stable state at finite T.

C. Freezing criterion for a discotic nematic fluid

The possibility of a freezing transition occurring in a dense nematic system can be analyzed from the static structure factor $S(\mathbf{k})$ of a nematic liquid (see the Appendix for a microscopic definition). In a first approximation, we can use the Ornstein-Zernike (OZ) equation for isotropic fluids and the formally exact expression,[37]

$$S(\mathbf{k}) = [1 - \rho \hat{c}(\mathbf{k})]^{-1}, \tag{11}$$

where the key ingredient is the Fourier transform of the direct two-point correlation function $c(\mathbf{r})$. For anisotropic particles this quantity will depend also on the particle orientations. A simple and tractable expression for the direct correlation function of a nematic fluid can be obtained from the Onsager-Parsons theory.[6,52–54] If we assume the platelets to be oriented parallel to the nematic director $\hat{\mathbf{n}}$, then $\hat{c}(\mathbf{k})$ takes the form of a cosine transform of the Mayer function Φ_M with a density

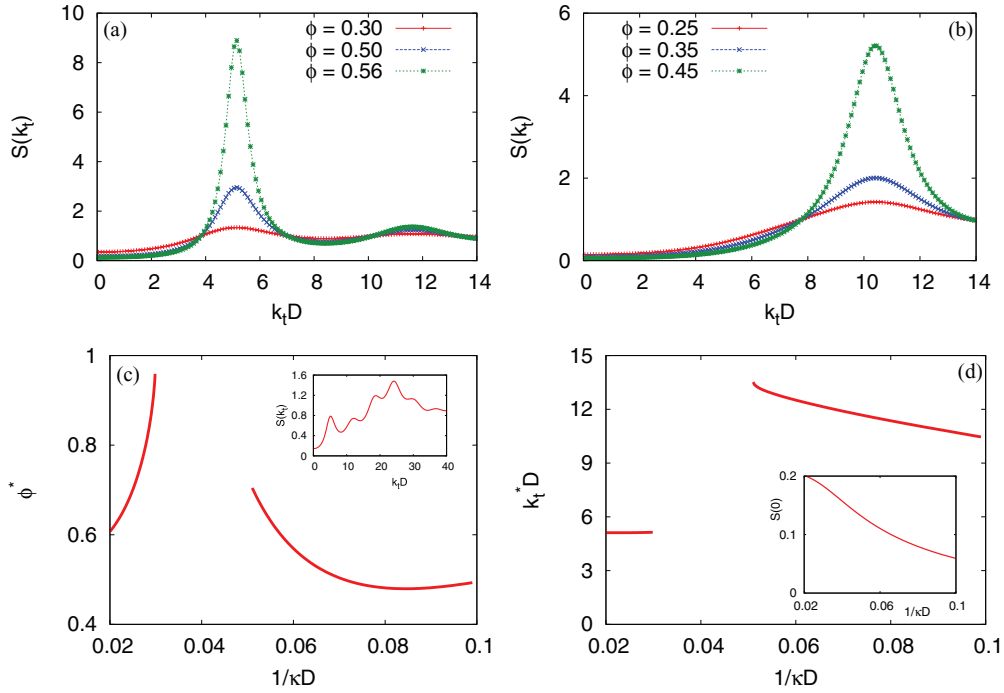

FIG. 5. Static structure factor of a dense nematic fluid from Onsager-Parsons theory. (a) Hard cylindrical platelets with $L/D = 0.05$. (b) Charged cylindrical platelets with $Z = 100$, $\lambda_B/D = 0.00233$, and $1/\kappa D = 0.1$ ($c_{salt} = 10^{-4}$ M). (c) Packing fraction at which a nematic-columnar bifurcation occurs as a function of the Debye length. The inset shows the structure factor for $1/\kappa D = 0.03$ ($c_{salt} = 10^{-3}$ M) and $\phi = 0.6$. The wavenumber corresponding to the nematic-columnar bifurcation is shown in (d). Inset: Osmotic compressibility versus Debye length for charged platelets with packing fraction $\phi = 0.45$.

-dependent prefactor:[55,56]

$$\hat{c}(\mathbf{k}) = g_P(\phi) \int d\mathbf{r} \Phi_M(\mathbf{r}) \cos(\mathbf{k} \cdot \mathbf{r}) \tag{12}$$

with $\Phi_M(\mathbf{r}) = \exp[-\beta U(\mathbf{r})] - 1$ and $g_P(\phi) = (1 - 0.75\,\phi)/(1-\phi)^2$ a prefactor arising from Parsons decoupling approximation for hard anisotropic particles (see, e.g., Ref. 57). If we assume the platelets to have a cylindrical shape we may invoke cylindrical coordinates to express the direct correlation function in case of 2D transverse density modulations with $\mathbf{k}_t \perp \hat{\mathbf{n}}$ as follows:[55]

$$\hat{c}(k_t) = -g_P(\phi)\pi L D^2 \frac{J_1(k_t D)}{\frac{1}{2}k_t D} + \int_0^\infty dr\, r J_0(k_t D r) \times \int_0^\infty dz \Phi_M\left(\sqrt{r^2+z^2}\right) \times [1 - \Theta(D-r)\Theta(L-z)], \tag{13}$$

where $J_n(x)$ represent standard Bessel functions and $\Theta(x)$ denote the Heaviside step function. The first term in Eq. (13) represents the contribution due to the cylindrical hard core whereas the second part takes into account the Yukawa potential in Eq. (4).

Instabilities of the nematic fluid with respect to transverse (columnar) density modulations can be probed from a divergence of the static structure factor $S^{-1}(k_t^*) = 0$ at some critical wavevector k_t^*. The results in Fig. 5 show that a dense fluid of hard platelets exhibits a main structure peak around $k_t D \sim 5$ with a pronounced sharpening occurring at larger packing fractions. The nematic-columnar instability occurs at $\phi^* = 0.583$ ($k_t^* D = 5.136$) which is beyond the nematic-columnar transition ($\phi \approx 0.40$) found in simulation. This overestimation must be attributed to the approximate nature of the Onsager-Parsons theory.

The results for the charged system (Fig. 5(b)) reveal a number of interesting features. For the salt concentration explored in the simulation (10^{-4} M) the structure factor exhibits a peak at much larger wavenumbers compared to the hard particle system. An overview of the instability of the nematic phase with respect to columnar density modulations is depicted in Figs. 5(c) and 5(d) for a range of screening lengths. At very high salt concentration ($1/\kappa D \ll 1$) the columnar structure strongly resembles that of the hard system with a typical intercolumnar spacing of about $2\pi/k_t^* D \approx 1.22$ times the platelet diameter. At low salt concentrations ($1/\kappa D \sim 0.1$, $c_{salt} \sim 10^{-4}$ M) the wavenumber of the columnar density modulations is located in the range $k_t^* D \sim 10$–13 which corresponds to intercolumnar spacings of about $0.5 - 0.6$ D, akin to the interdigitated columnar structures shown in Fig. 3.

In the intermediate regime of salt concentrations ($1/\kappa D \sim 0.04$, $c_{salt} \sim 10^{-3}$ M) the structure factor does not exhibit any pole and no columnar freezing instabilities occur. In this regime the structure factor tends to be very dispersed with a dominant peak at large wavenumbers (see Fig. 5(c)). Whether this particular feature can be connected to the formation of "stacked" structures observed at higher salt concentration $c_{salt} \sim 10^{-3}$ M (Fig. 3) remains an open question. It suffices to remark that it is conceivable that such a columnar nematic structure could emerge from a nematic fluid as the result

of a number of density modulations competing at different wavenumbers.

Finally, the structure factor can be connected to the isothermal osmotic compressibility χ_T in the zero-wavenumber limit[37]

$$\lim_{k_t \to 0} S(k_t) = \rho k_B T \chi_T \tag{14}$$

from which we can establish that the nematic fluid becomes less compressible upon increasing the Debye screening length as expected (see Fig. 5(d)).

It is important to bear in mind that the approach followed here is limited, since a rigorous analysis requires the introduction of the orientational degrees of freedom of the particles when the full OZ equation and correlation functions are used, according to theories developed in this direction.[58,59]

V. CONCLUSIONS

We have examined the phase behavior and microstructure of systems of charged colloidal platelets in an effort to elucidate the role of electrostatic interactions in systems of like-charged clay particles. The particle interactions are represented by a sterical hard cut-sphere interaction supplemented with an effective screened Coulomb potential. Simulation results reveal a marked shift in the isotropic-nematic transition induced by the soft electrostatic repulsions. The positional structure of the charged platelets is found to be very similar in the isotropic and nematic fluid phases whereas markedly different structures are found for the hard cut-sphere reference system.

At high pressures, anomalous hexagonal columnar order is found, characterized by interpenetrating columns and a strongly reduced intercolumnar spacing. These so-called interdigitated structures have also been observed in Gay-Berne models for (molecular) discotic mesogens with imbedded dipoles oriented within the molecular plane or along the disk normal.[60,61] At higher salt concentrations, disordered string-like structures are found, strongly reminiscent of the "columnar nematic" textures found in model gibbsite platelets.[30] String formation is well-known from dipolar spheres[62,63] and dipolar hard-spherocylinders[64] but has also been observed for confined plate-like colloids[65] and granular dipolar disks.[66] Rigid mineral clay particles such as kaolinite are also known to form compact stacked clusters (so-called "booklets") due to strong face-to-face attractions.[67] We remark that modeling gel forming clays such as kaolinite or laponite requires an accurate representation of the rim and face charges as well as incorporating attractive van der Waals forces[16,20] which goes beyond the scope of the present study.

Our study shows that the anomalous features of the columnar structure, i.e., interdigitation and columnar nematic order, can be generated by purely repulsive interactions only. It is at present unclear whether the columnar nematic structures represent true equilibrium states. Judging from the slow evolution of the structural properties at these high densities it is conceivable that these structures represent dynamically arrested, glassy states which are trapped in local minima of the free energy landscape. A careful examination of the dynamical properties of charged disks at high densities will hopefully clarify this issue.

ACKNOWLEDGMENTS

This project was supported by CONACYT (México) through Grant No. 61418 and a Ph.D. scholarship (LMA). An additional grant by CONACYT (Becas Mixtas Program) allowed LMA to spend a one-year academic research at Imperial College at Professor Galindo's group. H.H.W. acknowledges the Ramsay Memorial Fellowship Trust and the SFB-TR6 network for financial support. The authors would like to thank Henk Lekkerkerker (The Netherlands) and Ramón Castañeda-Priego (México) for fruitful discussions and for stimulating our interest in this problem. We also acknowledge Beatriz Millán (CFATA-UNAM, México) and high performance computing facilities provided by UNAM (Kambalam system).

APPENDIX: STATIC STRUCTURE FACTOR OF CYLINDRICAL DISKS

The static structure factor $S(\mathbf{k})$ can directly be measured in laser light scattering experiments. It is defined by[51]

$$S(\mathbf{k}) = \frac{1}{NP(\mathbf{k})} \left\langle \sum_{\alpha,\beta=1;\alpha\neq\beta}^{N} \exp[i\mathbf{k}\cdot(\mathbf{r}_\alpha - \mathbf{r}_\beta)] f_\alpha(\mathbf{k}) f_\beta(\mathbf{k}) \right\rangle, \tag{A1}$$

where $\mathbf{k}$ represents the scattering vector. The function $P(\mathbf{k})$ is the form factor of a colloidal platelet with homogeneous mass density; it depends only on the particle shape and is given by

$$P(\mathbf{k}) = \langle |f_\alpha(\mathbf{k})|^2 \rangle \tag{A2}$$

in which the brackets denote a canonical (orientational) average and $f_\alpha(\mathbf{k})$ represents a Fourier integral over a cylindrical disks with diameter D, thickness L, and orientational unit vector $\hat{\mathbf{u}}_\alpha$:

$$f_\alpha(\mathbf{k}) = \frac{\pi}{2} L D^2 \left(\frac{J_1(D\mathbf{k}\cdot\hat{\mathbf{w}}_\alpha/2)}{D\mathbf{k}\cdot\hat{\mathbf{w}}_\alpha/2} \right) \left(\frac{\sin(L\mathbf{k}\cdot\hat{\mathbf{u}}_\alpha/2)}{L\mathbf{k}\cdot\hat{\mathbf{u}}_\alpha/2} \right) \tag{A3}$$

with $J_1(x)$ a Bessel function of the first kind and $\hat{\mathbf{w}}_\alpha$ an (arbitrary) orientational unit vector perpendicular to $\hat{\mathbf{u}}_\alpha$.

[1] D. Frenkel and R. Eppenga, Phys. Rev. Lett. **49**, 1089 (1982).
[2] J. A. C. Veerman and D. Frenkel, Phys. Rev. A **45**, 5632 (1992).
[3] R. Blaak, D. Frenkel, and B. M. Mulder, J. Chem. Phys. **110**, 11652 (1999).
[4] N. Ibarra-Ávalos, A. Gil-Villegas, and A. Martínez-Richa, Mol. Simul. **33**, 505 (2007).
[5] F. M. van der Kooij, D. van der Beek, and H. N. W. Lekkerkerker, J. Phys. Chem. B **105**, 1696 (2001).
[6] L. Onsager, Ann. N.Y. Acad. Sci. **51**, 627 (1949).
[7] P. D. Duncan, M. Dennison, A. J. Masters, and M. R. Wilson, Phys. Rev. E **79**, 031702 (2009).
[8] R. P. S. Fartaria and M. B. Sweatman, Chem. Phys. Lett. **478**, 150 (2009).
[9] M. Marechal, A. Cuetos, B. Martínez-Haya, and M. Dijkstra, J. Chem. Phys. **134**, 094501 (2011).
[10] A. Cuetos and B. Martínez-Haya, J. Chem. Phys. **129**, 214706 (2008).
[11] H. H. Wensink and H. N. W. Lekkerkerker, Mol. Phys. **107**, 2111 (2009).
[12] H. van Olphen, *An Introduction to Clay Colloid Chemistry* (Wiley, New York, 1963).
[13] A. Mourchid, A. Delville, J. Lambard, E. Lecolier, and P. Levitz, Langmuir **11**, 1942 (1995).

[14]P. F. Luckham and S. Rossi, Adv. Colloid Interface Sci. **82**, 43 (1999).
[15]G. Odriozola, M. Romero-Bastida, and F. de J. Guevara-Rodríguez, Phys. Rev. E **70**, 021405 (2004).
[16]S. Kutter, J.-P. Hansen, M. Sprik, and E. Boek, J. Chem. Phys. **112**, 311 (2000).
[17]E. Trizac, L. Bocquet, R. Agra, J.-J. Weis, and M. Aubouy, J. Phys.: Condens. Matter **14**, 9339 (2002).
[18]M. Dijkstra, J. P. Hansen, and P. A. Madden, Phys. Rev. Lett. **75**, 2236 (1995).
[19]M. Dijkstra, J. P. Hansen, and P. A. Madden, Phys. Rev. E **55**, 3044 (1996).
[20]D. Léger and D. Levesque, J. Chem. Phys. **116**, 2251 (2002).
[21]S. Orlandi, L. Muccioli, M. Ricci, R. Berardi, and C. Zannoni, Chem. Cent. J. **1**, 15 (2007).
[22]L. J. Michot, I. Bihannic, S. Maddi, S. S. Funari, C. Baravian, P. Levitz, and P. Davidson, Proc. Natl. Acad. Sci. U.S.A. **103**, 16101 (2006).
[23]E. Paineau, K. Antonova, C. Baravian, I. Bihannic, P. Davidson, I. Dozov, M. Impéror-Clerc, P. Levitz, A. Madsen, F. Meneau, and L. J. Michot, J. Phys. Chem. B **113**, 15858 (2009).
[24]D. van der Beek and H. N. W. Lekkerkerker, Langmuir **20**, 8582 (2004).
[25]S. Liu, J. Zhang, N. Wang, W. Liu, C. Zhang, and D. Sun, Chem. Mater. **15**, 3240 (2003).
[26]A. B. D. Brown, S. M. Clarke, and A. R. Rennie, Langmuir **14**, 3129 (1998).
[27]M. C. D. Mourad, J. E. G. J. Wijnhoven, D. D. van't Zand, D. van der Beek, and H. N. W. Lekkerkerker, Philos. Trans. R. Soc. London, Ser. A **364**, 2807 (2006).
[28]M. C. D. Mourad, D. V. Byelov, A. V. Petukhov, and H. N. W. Lekkerkerker, J. Phys.: Condens. Matter **20**, 494201 (2008).
[29]M. C. D. Mourad, A. A. Verhoeff, D. V. Byelov, A. V. Petukhov, and H. N. W. Lekkerkerker, J. Phys.: Condens. Matter **21**, 474218 (2009).
[30]M. C. D. Mourad, D. V. Byelov, A. V. Petukhov, D. A. M. de Winter, A. J. Verkleij, and H. N. W. Lekkerkerker, J. Phys. Chem. B **113**, 11604 (2009).
[31]G. C. Ganzenmüller and G. N. Patey, Phys. Rev. Lett. **105**, 137801 (2010).
[32]C. Avendaño, A. Gil-Villegas, and E. González-Tovar, J. Chem. Phys. **128**, 044506 (2008).
[33]C. Avendaño, A. Gil-Villegas, and E. González-Tovar, Chem. Phys. Lett. **470**, 67 (2009).
[34]G. Jiménez-Serratos, C. Avendaño, A. Gil-Villegas, and E. González-Tovar, Mol. Phys. **109**, 27 (2011).
[35]R. Agra, E. Trizac, and L. Bocquet, Eur. Phys. J. E **15**, 345 (2004).
[36]M. Askari and J. Abouie, J. Phys.: Condens. Matter **23**, 155103 (2011).
[37]J. P. Hansen and I. R. McDonald, *Theory of Simple Liquids* (Academic, New York, 2006).
[38]D. G. Rowan, J.-P. Hansen, and E. Trizac, Mol. Phys. **98**, 1369 (2000).
[39]J. Dobnikar, R. Castañeda-Priego, H. H. von Grünberg, and E. Trizac, New J. Phys. **8**, 277 (2006).
[40]R. Castañeda-Priego, L. F. Rojas-Ochoa, V. Lobaskin, and J. C. Mixteco-Sánchez, Phys. Rev. E **74**, 051408 (2006).
[41]E. Trizac, L. Belloni, J. Dobnikar, H. H. von Grünberg, and R. Castañeda-Priego, Phys. Rev. E **75**, 011401 (2007).
[42]L. F. Rojas-Ochoa, R. Castañeda-Priego, V. Lobaskin, A. Stradner, F. Scheffold, and P. Schurtenberger, Phys. Rev. Lett. **100**, 178304 (2008).
[43]J. M. Falcón-González and R. Castañeda-Priego, J. Chem. Phys. **133**, 216101 (2010).
[44]J. M. Falcón-González and R. Castañeda-Priego, Phys. Rev. E **83**, 041401 (2011).
[45]A. Gil-Villegas, A. Galindo, and G. Jackson, Mol. Phys. **99**, 531 (2001).
[46]A. Ortega-Rodríguez, S. A. Cruz, A. Gil-Villegas, F. Guevara-Rodríguez, and C. Lira-Galeana, Energy Fuels **17**, 1100 (2003).
[47]D. van der Beek, T. Schilling, and H. N. W. Lekkerkerker, J. Chem. Phys. **121**, 5423 (2004).
[48]S. D. Zhang, P. A. Reynolds, and J. S. van Duijneveldt, J. Chem. Phys. **117**, 9947 (2002).
[49]M. M. Piñeiro, A. Galindo, and A. O. Parry, Soft Matter **3**, 768 (2007).
[50]M. P. Allen, G. T. Evans, D. Frenkel, and B. M. Mulder, Adv. Chem. Phys. **86**, 1 (1993).
[51]T. Kirchhoff, H. Löwen, and R. Klein, Phys. Rev. E **53**, 5011 (1996).
[52]J. D. Parsons, Phys. Rev. A **19**, 1225 (1979).
[53]S. D. Lee, J. Chem. Phys. **87**, 4972 (1987).
[54]S. D. Lee, J. Chem. Phys. **89**, 7036 (1989).
[55]B. M. Mulder, Phys. Rev. A **35**, 3095 (1987).
[56]H. H. Wensink, J. Chem. Phys. **126**, 194901 (2007).
[57]S. C. McGrother, D. C. Williamson, and G. Jackson, J. Chem. Phys. **104**, 6755 (1996).
[58]H. Workman and M. Fixman, J. Chem. Phys. **58**, 5024 (1973).
[59]H. Zhong and R. F. Petschek, Phys. Rev. E **51**, 2263 (1995).
[60]R. Berardi, S. Orlandi, and C. Zannoni, J. Chem. Soc., Faraday Trans. **93**, 1493 (1997).
[61]R. Berardi, S. Orlandi, and C. Zannoni, Liq. Cryst. **32**, 1427 (2005).
[62]K. Butter, P. H. H. Bomans, P. M. Frederik, G. J. Vroege, and A. P. Philipse, Nature Mater. **2**, 88 (2003).
[63]C. Holm and J. J. Weis, Curr. Opin. Colloid Interface Sci. **10**, 133 (2005).
[64]A. Gil-Villegas, S. C. McGrother, and G. Jackson, Chem. Phys. Lett. **269**, 441 (1997).
[65]A. Satoh and Y. Sakuda, Mol. Phys. **108**, 2105 (2010).
[66]P. Coutiño, N. Ibarra-Ávalos, and A. Gil-Villegas, Rev. Mex. Fís. **56**, 435 (2010).
[67]J. P. Olivier and P. Sennett, *Clays and Clay Minerals* (Pergamon, New York, 1973), Vol. 21.